The Effect of Flow on CO_2 Corrosion of Self-Healing Metallic Coatings

Jonathan Prout
National Energy Technology Laboratory
1450 Queen Avenue SW
Albany, OR 97321
USA
Oak Ridge Institute for Science and Education
299 Bethel Valley Road
Oak Ridge, TN 37830
USA

Zineb Belarbi
National Energy Technology Laboratory
1450 Queen Avenue SW
Albany, OR 97321
USA
NETL Support Contractor
1450 Queen Avenue SW
Albany, OR 97321
USA

Ömer Doğan
National Energy Technology Laboratory
1450 Queen Avenue SW
Albany, OR 97321
USA

ABSTRACT

Internal corrosion is an issue that affects natural gas pipelines, a significant part of the United States' energy infrastructure. Over time, this corrosion has worn away longstanding pipelines due to the original construction materials used for the lines and impurities in the gas and liquid streams flowing through them. The main impurities in natural gas are H_2O, CO_2, H_2S, and O_2. One of the leading causes of corrosion is the CO_2 dissolved in water, giving rise to carbonic acid formation, which can further dissolve the steel pipe. The National Energy Technology Laboratory (NETL) has been studying different solutions to this problem. One potential answer is a self-healing sacrificial metallic coating applied by a novel cold spray technique. Previous studies at NETL have shown that the zinc-rich, self-healing coating can withstand corrosion through passivation and create a barrier to the diffusion of corrosive species. This study explored the impact of flow on corrosion with this coating and carbon steel when exposed to a saturated CO_2 environment by simulating the pipeline flow profile in a small-scale lab setting. The samples were evaluated using multiple electrochemical techniques that found corrosion rates and were backed up with surface analysis to conclude the behavior of the corrosion mechanisms. The cold spray coating exhibited steel corrosion protection under flow conditions. This study has significantly advanced our understanding of CO_2 corrosion, particularly in the context of natural gas pipelines and coating design. The findings have practical implications for the future, providing valuable insights that can be applied to developing more effective coatings and maintaining pipeline integrity.

Key words: CO_2 corrosion, natural gas pipelines, cold spray, internal coatings, carbon steel, flow

INTRODUCTION

Internal corrosion is an issue that affects natural gas pipelines, a significant part of the United States' energy infrastructure. Over time, this corrosion has worn away at longstanding pipelines due to the original construction materials used for the lines and impurities in the gas and liquid streams flowing through them. In a survey done by the National Energy Technology Laboratory (NETL), 112 (12%) of the incidents reported to cause failures in transmission lines across the U.S. for eight years were due to internal corrosion (Figure 1)[1,2]. Transmission lines deliver the natural gas long distances, often across multiple states, from gathering systems to refining, processing, or storage facilities. Some refinement is done at the source, but some impurities in low quantities make it into these transmission lines and are enough to cause internal corrosion. The main impurities in natural gas are H_2O, CO_2, H_2S, and O_2. One of the leading causes of corrosion is the CO_2 dissolved in water, giving rise to carbonic acid formation, which can further dissociate and release CO_3^{2-}, HCO_3^-, and an extra amount of H^+ that acidifies the medium and causes the dissolution of steel[3-6]. The corrosion mechanism in the sweet gas environment is CO_2-dominated, and iron carbonates are the main corrosion product[7].

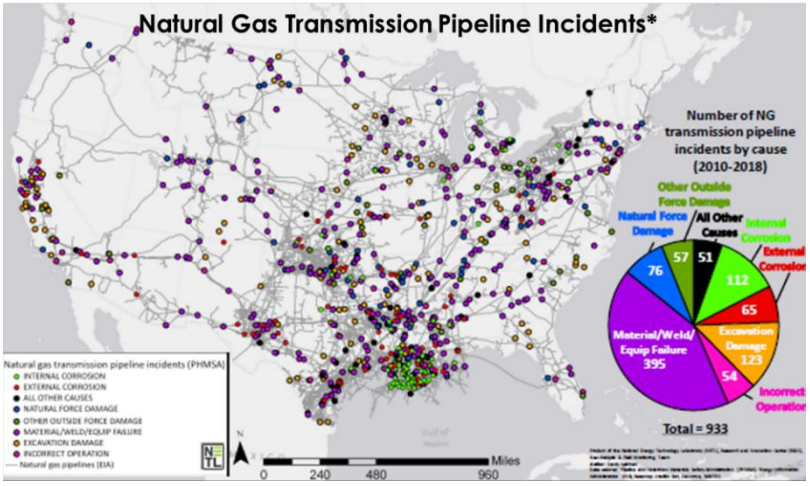

Figure 1: NETL performed an incident survey from 2010 through 2018 and found that 112 (12%) of these incidents were caused by internal corrosion.

Several methods have been suggested to combat pipeline corrosion. Inhibitors have been used for various types of corrosion in different pipe streams; however, they are mainly added by mixing them into the liquid phases of pipes[4,5,8,9]. This creates an issue with natural gas transmission lines, as they consist primarily of a gas stream, which makes it hard to distribute the inhibitors to all areas of the pipe. Coatings are one of the most widely used solutions to slow internal corrosion. Some coatings, such as polymer-based materials[10,11] have shown issues with flow shear stress resistance, short life, or localized pitting corrosion in application[12]. Cold spray technology is a novel coating technology primarily used in military vehicle applications and marine environment protection[12]. Due to its good coating properties, it is being proposed as a corrosion protection system. The cold spray technique is applied mechanically using metallic particles, creating a dense coating. This can help lead to less localized corrosion and penetration through the coating. The proposed coating in this study can also act as a self-healing coating as it can create a passivated layer of corrosion on the damaged regions of the coating, stopping further corrosion[13]. Recent research published by Belarbi et al.[13] showed that zinc cold spray metallic coatings can protect natural gas pipelines and equipment from internal corrosion. The authors investigated the corrosion resistance of ZnCr and ZnNb coatings in 3.5 wt.% NaCl saturated with CO_2[13,14] and in a live natural gas pipeline transporting wet natural gas out of an underground storage well at the Northwest Natural gas storage facility in Mist, Oregon[15,16]. It was found that ZnNb's excellent corrosion resistance is attributed

to the synergy between the cathodic protection provided by the sacrificial coatings (ZnNb) and the zinc carbonate layer on the surface that inhibits further diffusion of corrosive species into the coating[13,15,16]. Internal corrosion via dissolved CO_2 is affected by many parameters, including pH, potential, solubility, temperature, and flow. This study aims to determine the effect flow has on corrosion in natural gas pipelines and the proposed coating resistance to corrosion. This study will isolate CO_2 as the primary contributor to corrosion via a saturated aqueous solution so that these effects can be separately assigned to what happens in transmission lines with other impurities. Transmission pipelines are primarily operated in turbulent flow regimes at up to 5×10^7 Reynolds number [17,18]. This depends on the gas velocity, pipe diameter, and viscosity. Many researchers investigated the effect of flow on pipeline CO_2 corrosion, and they found that an increase in flow may lead to an increase in the corrosion rate in cases where protective scales do not form, typically at a low pH environment ($3 < pH < 5$)[19]. In this case, turbulent flow's primary role is to enhance species' transport toward and away from the metal surface. However, when protective iron carbonate scales form at higher pH environments ($3 < pH < 5$), the flow interferes with the formation of scales or removes the deposited scales from the surface, which leads to an increase in corrosion rate[20]. Removing a protective surface scale of iron carbonate may occur under multiphase flow conditions, particularly unsteady slug flow, when significant short-lived fluctuations in the wall-shear stress are present, which can lead to the onset of localized attack[3].

This paper used a mass transfer characterization to develop a lab equivalent to the specific velocity profile and simulate the natural gas transmission line flow profile. Multiple electrochemical techniques were used to study the coating system because they have shown dynamic results, giving interpretations of most aspects of the corrosion process. The main methods used were potentiodynamic polarization (PDP), open circuit potential (OCP), linear polarization resistance (LPR), and electrochemical impedance spectroscopy (EIS). To study the physical features further, the surface was analyzed and characterized using scanning electron microscopy (SEM) and energy-dispersive X-ray spectroscopy (EDS).

EXPERIMENTAL PROCEDURE

MATERIALS AND CHEMICALS

The samples used for the experiment were machined into circular discs from a larger flat sheet of mild steel USN G10180 coated with a cold-sprayed ZnNb. This paper will not present the conditions of the cold spray process for confidentiality reasons. The porosity and the thickness of ZnNb cold spray coating are approximately $0.32 \pm 0.13\%$ and 900 µm, respectively. The wavelength dispersive X-ray fluorescence analysis (WDXRF) of ZnNb cold spray coating showed that the coating contains 0.69 wt.% Nb, with zinc balance. The X-ray diffraction (XRD) analysis revealed the presence of elements Zn and Nb, and no intermediate phases were detected. Uncoated UNS G10180 steel was used for corrosion testing as a baseline to compare to the coating under the same testing conditions. The electrolyte used for electrochemical testing was 3.5 wt.% NaCl aqueous solution saturated with CO_2 gas via sparger for at least 2 hours before use. Deoxygenated equimolar aqueous solutions of 0.01M $K_3(Fe(CN)_6$ and $K_4Fe(CN)_6 \cdot 6H_2O$ in 0.5 M of NaOH were used as the electrolyte to characterize the mass transport and obtain a mass transfer coefficient characteristic of the impeller configuration in Figure 2.

ELECTROCHEMICAL MEASUREMENTS

The mass transport characteristics of the experimental setup shown in Figure 2 were initially characterized before corrosion tests. All tests were done in an enclosed standard three-electrode glass cell, as seen in Figure 2. The cell involved a Saturated Calomel Electrode (SCE) as the reference electrode, a graphite rod as the counter electrode, and the working electrode. The mass transport was characterized using a stainless steel 316 with an area of 1 cm^2 as the working electrode on the ferri-ferrocyanide coupled reaction (Equation 1). Before each experiment, the working electrode surface was polished with silicon carbide paper (320, 400, and 600 grit), sonicated in isopropanol for 5 minutes to remove residual deposits, and air-dried before immersion in the cell. The experimental procedure to identify mass transport has been detailed in previous studies[21]. Deoxygenated equimolar aqueous solutions of 0.01 M $K_3(Fe(CN)_6$ and $K_4Fe(CN)_6 \bullet 6H_2O$ in 0.5 M of NaOH were used as the electrolyte. A

significant excess of sodium hydroxide was used to eliminate the contribution of ionic migration to mass transfer, and the solutions were kept in the dark to mitigate slow decomposition in light[21]. This study used an impeller with a diameter of 3.95 cm. Voltammetry was conducted from 0.155 V vs. SCE to -1.345 V vs. SCE at a scan rate of 5 mV/s. Flow was controlled between 0 and 1,000 rpm at room temperature (23 °C) and 40 °C. The tests were repeated to ensure the repeatability of the measurement technique and the experimental apparatus. After the voltammogram was obtained, the average limiting density at the plateau portion of the cathodic curves was used to calculate the mass transfer coefficient using Equation 2. Equation 2 does not consider the contribution of ionic migration to mass transfer due to the excess of NaOH in the electrolyte. [21].

$$[Fe(CN)_6]^{3-} + e^- \rightleftarrows [Fe(CN)_6]^{4-} \quad (1)$$

$$\frac{I_{lim}}{nF} \approx C_b k_m \quad (2)$$

Where I_{lim} is the limiting current in A/m^2, n is the number of moles of electrons transferred between reductant and oxidant in mol electrons/mol (1 as shown in Equation 1), F is Faraday's constant in C/mol electrons, C_b is the concentration of the active species in mol/m^3, and k_m is the mass transfer coefficient in m/s. The mass transfer coefficient and the system's geometry can be used to calculate relevant dimensionless numbers (Sherwood, Reynolds, and Schmidt) that characterize the flow hydrodynamics of the system using Equations 3-5 below.

$$Sh = \frac{k_m L}{D} \quad (3)$$

$$Re = \frac{uL}{\nu} \quad (4)$$

$$Sc = \frac{\nu}{D} \quad (5)$$

Where *Sh* is the Sherwood number, k_m is the mass transfer coefficient in m/s, *L* is the characteristic length in m, *D* is the temperature-adjusted diffusion coefficient in m^2/s, *Re* is the Reynolds number, *u* is the characteristic velocity in m/s, *v* is the temperature-adjusted kinematic viscosity in m^2/s, and *Sc* is the Schmidt number. Temperature-adjusted values for both *D* and *v* were obtained from the literature[21], while the characteristic length and velocity for the impeller are the diameter and peripheral velocity, respectively[21].

For corrosion studies and to avoid any oxygen contamination, before each test, the glass cell was saturated with CO_2 gas via sparger, as shown in Figure 2, before adding the electrolyte. To prevent the risk of oxygen gas in the cell from dissolving into the electrolyte, 90% of the volume was filled (2 liters). The electrolyte (3.5 wt.% NaCl aqueous solution saturated with CO_2) was kept at room temperature (23 °C) and atmospheric pressure (1 bar). As expected, the pH was 3.9 from pH probe readings before tests. The corrosion tests were performed on an uncoated and coated steel sample, with an exposed area of 0.19 cm^2, sealed inside a Teflon sample holder as the working electrode. Before each experiment, the specimen surface was polished with silicon carbide paper (600 grit), sonicated in isopropanol for 5 min to remove residual deposits, and air-dried before immersion in the cell. Testing was carried out with the Gamry 600 Plus model using Gamry software to control PDP, LPR, EIS, and measure the Open Circuit Potential (OCP). PDP test results were calculated by applying a direct signal (DC) potential with a scan rate of 1 mV/s starting at -0.6V to 1V vs. OCP, where each sample tested was duplicated. The LPR measurement was performed using a DC signal at -5 mV vs. OCP to +5 mV vs. OCP at 0.125 mV/s. The Tafel values (β_a and β_c) and the current density (i_{corr}) for these experiments were determined by Tafel's extrapolation method using Gamry or Origin software. The linear portions of the anodic and cathodic curves meet the OCP potential at the same point, giving the (i_{corr},) and the corrosion rate, which was calculated using Equation 6[13].

$$CR = K * \frac{i_{corr} * EW}{\rho} \quad (6)$$

The polarization resistance (R_p) extracted from LPR measurement was used to calculate corrosion current $I_{corr,}$ considering the Stern-Geary assumption (Equation 7)[13].

$$I_{corr} = \frac{1}{R_p} * \frac{\beta_a * \beta_c}{2.303(\beta_a + \beta_c)} \quad (7)$$

The corrosion rate (CR) for uniform corrosion was found to be a loss in length per year (mm/y). Equivalent weight (EW) in (g/equivalent), corrosion current density (i_{corr}) in A/cm^2, time constant/unit conversion factor (K) in (mm*g/A*cm*y), density (Rho) in (g/cm^3). The EIS measurements were determined by applying 10 mV (rms) alternating signal (AC) amplitude at OCP for points in the frequency range of 100 kHz to 0.10 mHz. For the EIS and LPR tests, data was seen through the following method: holding the cell in an initial 1-hour OCP hold, followed by LPR measurement, another 10-minute OCP hold, and finally, the EIS measurement. This method was looped for 14 cycles for each sample tested, lasting approximately 24 hours, and each test was duplicated. Samples were kept in nitrogen-enclosed desiccators during handling for preparation and observation to reduce any excess corrosion caused by the natural environment. All the tests were performed under stagnant conditions and turbulent flow (200 rpm equivalent to Reynolds's number of 5839).

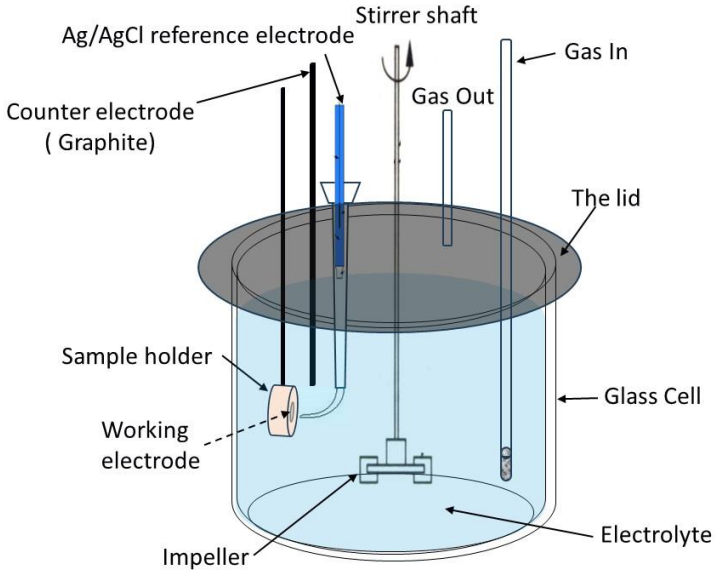

Figure 2: Image of standard three-electrode setup for mass transport characterization and electrochemical testing in a closed glass cell.

SURFACE ANALYSIS

Surface characterization was done via a SEM with EDS capability for microchemical analysis. Unexposed and corroded samples after 24 hours of exposure to 3.5 wt.% NaCl aqueous solution saturated with CO_2 were analyzed using SEM/EDS.

RESULTS

MASS TRANSPORT CHARACTERIZATION

The voltammogram collected for the impeller at room temperature in equimolar 0.01 M $K_3(Fe(CN)_6$ and $K_4Fe(CN)_6 \bullet 6H_2O$ in 0.5 M of NaOH is shown in Figure 3Figure **1**. At ambient (23 °C) and 40 °C, the limiting current density from the voltammogram increased as the controlled speed increased. Laminar flow occurs

for flow situations with a Reynolds number below 2,100 and turbulent flow with a Reynolds number above 4,000. The mass transfer coefficient (Km) and the Reynolds number (Re) were calculated using Equations 3 and 4. Figure 4 shows that the mass transfer coefficient increased linearly as the Reynolds number increased. Additional regression analyses yielded an empirical mass transfer correlation (Equation 8) for the impeller setup that combines the Sherwood, Reynolds, and Schmidt numbers.

$$Sh = 1.98Re^{0.56}Sc^{-0.47} \quad (8)$$

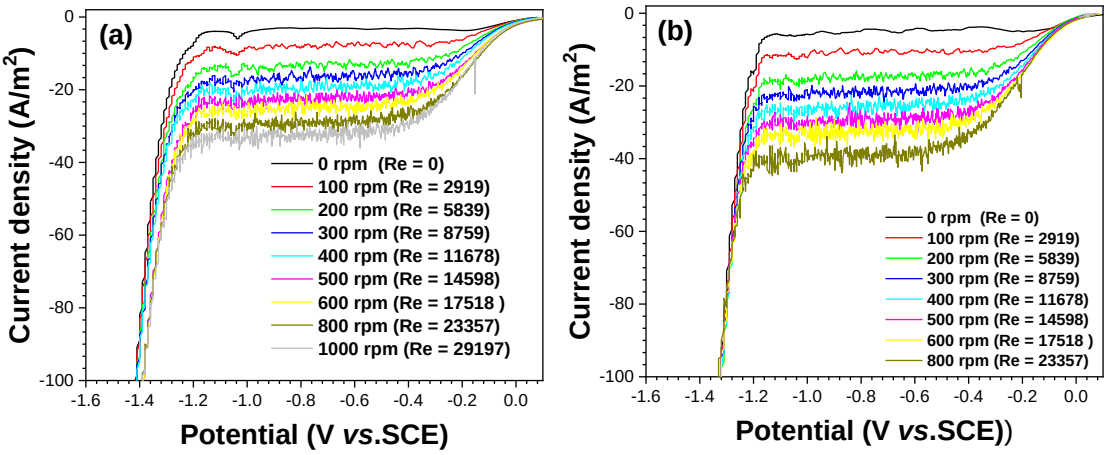

Figure 1: Cathodic polarization curves of ferricyanide ion reduction using impeller experimental setup described in **Error! Reference source not found.**: (a) at ambient temperature (23 °C), and (b) at and 40 °C.

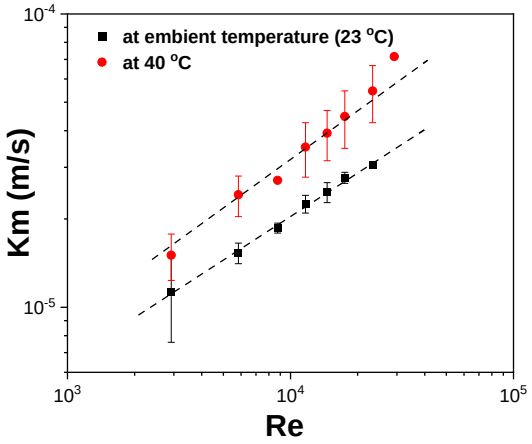

Figure 4: Mass transport and Reynolds number correlations for the impeller.

CORROSION TESTS: *POTENTIODYNAMIC POLARIZATION CURVE*

Figure 5 shows the results from the PDP experiments. The two main parts of these curves are the anodic, above the OCP, and the cathodic below the OCP regions. The anodic region is where species are oxidized, the dissolution of iron for uncoated steel (Equation 9), and the dissolution of zinc for coated steel with ZnNb (Equation 10). The cathodic region is where the hydrogen evolution occurs via the reduction of H+ (Equation 11) and water molecules. The corrosion mechanism of uncoated and coated steel has been explained in previous studies[13]. The initiation of CO_2 corrosion starts with the dissolution of CO_2 in water (Equation 12), giving rise to weak carbonic acid, which dissociates from carbonate ions and proton H^+ (Equations 13 and 14). The carbonate formation is seen when this carbonate ion reacts with the Zn or Fe ion, forming the product layer (Equation 15, 16).

$$Fe \overset{1}{\Leftrightarrow} Fe^{2+} + 2\,e^- \quad (9)$$

$$Zn \overset{1}{\Leftrightarrow} Zn^{2+} + 2\,e^{-} \quad (10)$$

$$2\,H^{+} + 2\,e^{-} \overset{1}{\Leftrightarrow} H_2 \quad (11)$$

$$CO_2 + H_2O \overset{1}{\Leftrightarrow} H_2CO_3 \quad (12)$$

$$H_2CO_3 \overset{1}{\Leftrightarrow} HCO_3^{-} + H^{+} \quad (13)$$

$$HCO_3^{-} \overset{1}{\Leftrightarrow} CO_3^{2-} + H^{+} \quad (14)$$

$$CO_3^{2-} + Fe^{2+} \overset{1}{\Leftrightarrow} FeCO_3 \quad (15)$$

$$CO_3^{2-} + Zn^{2+} \overset{1}{\Leftrightarrow} ZnCO_3 \quad (16)$$

The first thing to notice in Figure 5 is that under stagnant and flow conditions, the OCP of coated steel with ZnNb is more cathodic than that of uncoated steel. The flow shifted the corrosion potential to a more cathodic potential for uncoated carbon steel and increased the corrosion current density (Table 1). An increase in turbulent flow may lead to an increase in the corrosion rate due to the rise in the mass transport of species toward and away from the metal surface[19]. The hydrogen reduction is mainly dependent on the diffusion of free aqueous ions. This leads to the conclusion that more corrosion will be seen with the increased flow because of this mass diffusion-dependent reaction[19]. The uncoated steel had higher CR under the flow condition, which was expected from previous works[19]. However, for coated steel with ZnNb, the flow decreased the current density but did not affect the OCP; no shift of OCP was observed. The other important takeaway from this data is the magnitude of the CR values is close to what has been seen in previous studies for CO_2 corrosion on these types of metals[13]. Although the CR value at stagnant conditions of the coating showed a very high value of 20.07 mm/y, which was unexpected, it is only an estimated value of the initial 1 hour of exposure to these conditions. It should be noted that this relationship ignores the fact that localized corrosion can occur and not be uniform across the surface, but it should still be valid as an estimate for this project. Previous studies have shown flow profiles to cause a change in the corrosion reaction at the metal/liquid interface[19]. Findings from a field test study on ZnNb cold-sprayed coating in a pipeline carrying gas from a storage well showed that the coating demonstrated higher corrosion rates in flow conditions than in the stagnant pipeline[16]. The significant increase in mass diffusion due to the flow is likely causing the increased corrosion rates, which are also expected to be seen in this study. The corrosion kinetic parameters E_{corr}, i_{corr}, and CR for uncoated and coated carbon steel with Zn cold spray coatings are shown in Table 1.

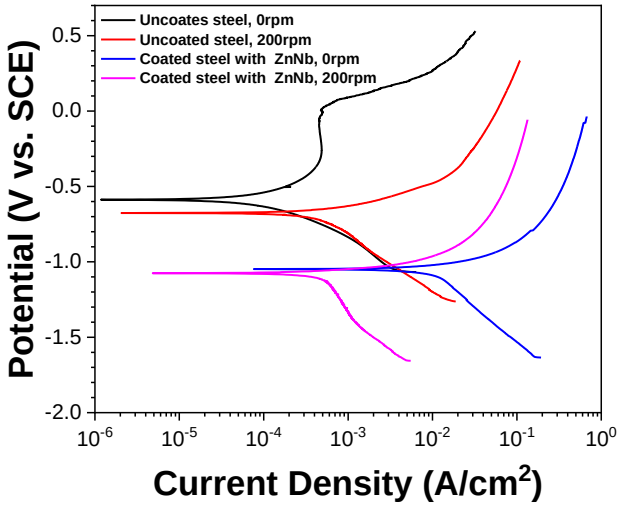

Figure 5: PDP curves of uncoated and coated steel with ZnNb in conditions with and without flow. This graph shows Potential (V vs. SCE) vs. Current Density (A/cm^2).

Table 1. Corrosion Kinetic Parameters E_{corr}, i_{corr}, and CR for the UNS G10180 and Carbon Steel Coated with Cold Spray Coating Immersed in a 3.5 wt.% NaCl Solution Saturated with CO_2 at 23 °C under Stagnant and Flow Conditions.

Alloys	E_{corr} (V vs.SCE)	i_{corr} (A/cm^2)	β_a (V/decade)	β_c (V/decade)	CR (mm/y)
Uncoated steel under stagnant conditions (0 rpm (Re =0))	-0.58	2.85×10^{-5}	0.057	0.056	0.33
Uncoated steel under flow conditions (200 rpm (Re =5,839))	-0.67	1.10×10^{-4}	0.037	0.051	1.28
Steel coated with ZnNb under stagnant conditions (0 rpm (Re =0))	-1.04	1.25×10^{-3}	0.049	0.058	18.57
Steel coated with ZnNb under flow conditions (200 rpm (Re =5,839))	-1.07	1.15×10^{-4}	0.021	0.054	1.71

LINEAR POLARIZATION RESISTANCE: CORROSION RATE

Figure 6 shows the results of the LPR tests and calculated CR values. All the initial values (first 2 hours) are similar and of the same magnitude as the CR values found from PDP estimations in Table 1. Without flow, the initial corrosion rate for uncoated steel was approximately 1.4 mm/y. After 1 hour of exposure, the CR increased to 1.67 mm/y, then after 12 hours of exposure, the CR decreased to a stable value of 0.8 mm/y. The increase in CR is due to the active dissolution of iron (Equation 11), which increases the pH (accelerate cathodic reaction, Equation 13) at the interface surface/electrolyte. Once the solution is supersaturated, $FeCO_3$ forms on the steel surface (Equation 17), slowing down the CR. With the flow, the CR of uncoated steel was approximately 0.8 mm/y. This could be due to the flow, which accelerated the dissolution of the steel and mass transport of the species to the surface, accelerating the formation of $FeCO_3$ on the steel sample (Equation 17) and slowing down the corrosion rate. This is in good agreement with what was seen in the literature[19]. Without flow, the initial corrosion rate for coated steel with ZnNb was approximately 17 mm/y. After 8 hours of exposure, the CR decreased to a stable value of 3.9 mm/y. The high CR is due to the formation of micro galvanic cells between Zn and Nb, accelerating the dissolution of zinc (Equation 12) and increasing the pH (accelerate cathodic reaction, Equation 13) at the interface surface/electrolyte. Once the solution is supersaturated, $ZnCO_3$ forms on the top of the coating (Equation 18). The same behavior was observed by Belarbi et al.[13]. The coating also showed similar results to uncoated steel, where the flow condition CR values were steadily lower (0.7 mm/y) than those without flow (4.9 mm/y). This could be due to the flow, which accelerated the dissolution of Zn and mass transport of the species to the surface, accelerating the formation of $ZnCO_3$ on the top of the coating (Equation 18) and slowing down the corrosion rate. The OCP graph in Figure 7 reveals the stability data of the uncoated and coated steel with ZnNb during 24 hours of immersion in 3.5 wt.% NaCl solution saturated with CO_2. Figure 7 indicates that carbon steel coated with ZnNb with (-1.10 V. vs. SCE) and without flow (-1.07 V. vs. SCE) has more noble potential values than uncoated steel.

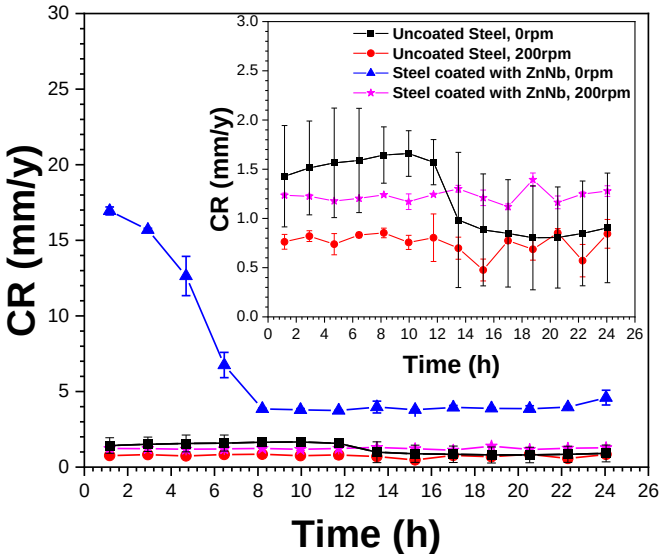

Figure 6: Corrosion rate (CR) (mm/y) vs. time (h) plot of uncoated and coated steel with ZnNb with and without flow.

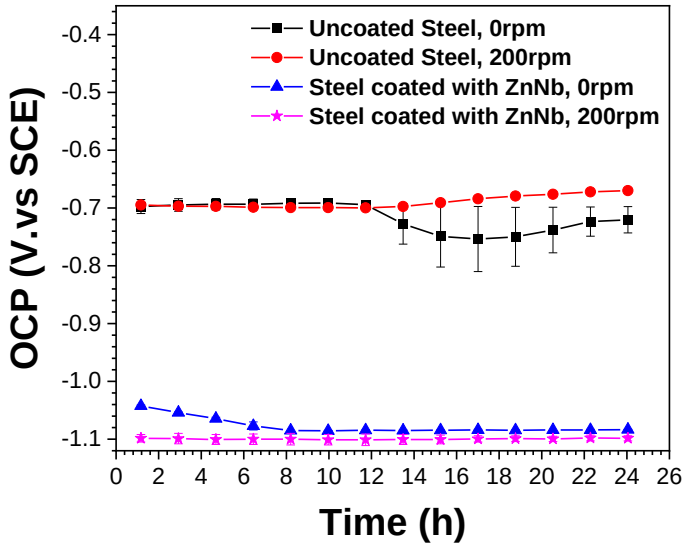

Figure 7: OCP (V vs. SCE) vs. time (hours) plot of uncoated and coated steel with ZnNb coating with and without flow.

ELECTROCHEMICAL IMPEDANCE SPECTROSCOPY

EIS measurements were carried out to complement the LPR results. Figure 8 shows the corrected Nyquist plots and Bode diagram, without the resistance of electrolytes, of uncoated and coated carbon steel with cold spray coatings (ZnNb) after 24 hours of exposure to 3.5 wt.% NaCl solution saturated CO_2 with and without flow (Figures 8a, 8 b). For uncoated steel and with and without flow, the EIS Nyquist curves (Figure 8 a) showed similar characteristics to the known corrosion behavior of bare steel[13]. The Nyquist diagram showed a depressed capacitive loop at high to medium frequencies, indicating a double-layer capacitance. Depressed semi-circles are characteristic of heterogeneous surface roughness and the non-uniform current density distribution on the surface[13]. The flow decreased the low-frequency limit of the impedance (Figure 8b) compared to uncoated steel without flow, indicating a decrease in corrosion rate, as shown in Figure 6. Coated steel with ZnNb cold spay coating showed a second-time constant, typical of a coating layer on the steel surface. The average solution resistance was estimated at approximately 40 Ohms. The impedance modulus value of samples exposed to flow was twice as high as the ones without flow (Figure 8b), indicating the decrease in corrosion rates due to the flow, which

accelerated the formation of scale on top of the surface. This agrees with the PDP and LRP results. In addition to the charge transfer process and the double-layer capacitance, a diffusion was observed in the low-frequency domain for coated steel with ZnNb. This can be attributed to the diffusion of the species through the corrosion product layer.

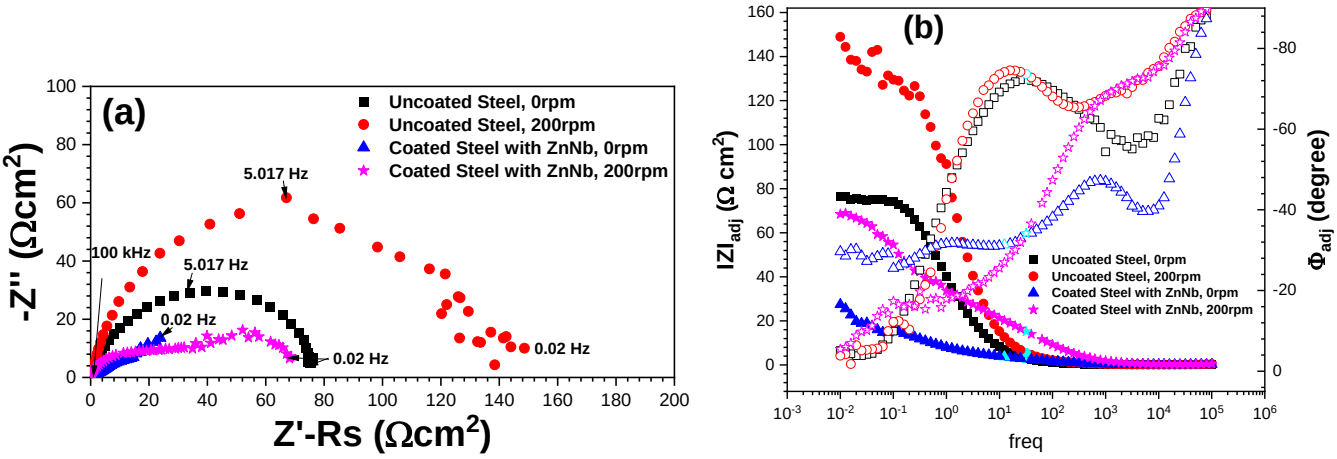

Figure 8: Nyquist diagrams (a) and Bode diagrams (modulus (■ ● ▲), phase angle (□ ○ Δ)) of uncoated and coated carbon steel with ZnNb cold spray coating immersed in a 3.5 wt.% NaCl solution saturated with CO_2 at 23 °C, after 24 hours with and without flow.

SURFACE CHARACTERIZATION

The surface characterization was organized in Figure 9, showing the original scan from the SEM on the left corresponding to the following EDS spectra taken on the right of each element found in each sample under both flow conditions. The SEM images from the backscattered electrons (BE) detector were taken at x500 magnification. Other magnifications were taken to confirm consistency throughout the samples; however, those are not shown here. The only samples imaged were post-24 hours of exposure to CO_2 aqueous corrosion environment and one of each unexposed metal to any corrosion conditions for a control comparison. For the uncoated steel samples, Fe, which was in the majority, Mn, and C were expected for all the conditions tested due to the makeup of the steel UNS G10180. Oxygen was found in all the exposed samples to corrosion conditions, including the ZnNb coating. Oxygen in corroded samples indicates that iron and zinc carbonates were possibly formed as corrosion products. However, this cannot be quantitatively confirmed until further analysis from other techniques, such as XRD, is done. Also, note that the steel corroded sample without flow had two unique types of morphologies, which may be identified as ferrite and pearlite microstructures of typical carbon steel[22]. This may cause uneven steel corrosion at the surface due to a mixture of these two structures, which initially corrode at different rates. The steel sample under the flow conditions showed a different morphology from the stagnant condition sample, which appeared disturbed by the flow, possibly indicating surface shearing. This would be expected with a turbulent flow, which would also give rise to a more significant corrosion rate as new exposed Fe is created from the flow. This could explain the increase in corrosion seen from the PDP curves for the flow condition. The ZnNb coating analysis from EDS exhibited Zn as the primary element and a small amount of carbon and Nb, as expected from the known coating formulation. Oxygen was again only present in the exposed corroded samples seen in Figure 8, indicating the possible formation of $ZnCO_3$ as a corrosion product. The other important finding from the EDS was the absence of Fe in all coated samples measured. This confirms that the coating layer was still intact throughout the sample. The morphology of the coated sample under no flow conditions was much different than the unexposed sample and looked deformed, indicating corrosion occurred. The type of corrosion on the coated samples seen from SEM imaging seemed to be uniform, as no pitting was found. When exposed to the flow conditions, the coating also had a different surface, but it did not exhibit the same type of “shearing” seen in the previous uncoated steel sample exposed to flow. This may suggest that after the carbonate layer formed, it passivated quickly and remained intact on the surface to help create the barrier to further

corrosion. This would explain the lower corrosion seen from the coating when exposed to flow than in stagnant conditions.

	Original Image	Primary Metal: Iron/Zn	Minor Metal: Mn/Nb	C	O
Unexposed Bare Steel	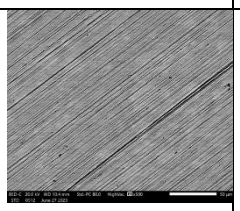	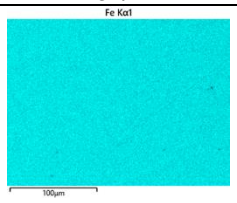	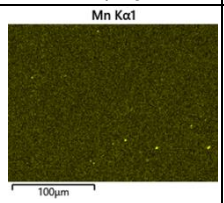	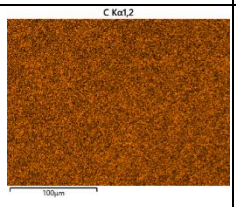	None Present
Unexposed ZnNb Coating	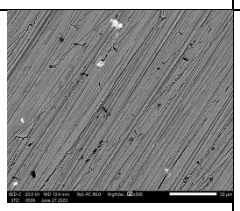	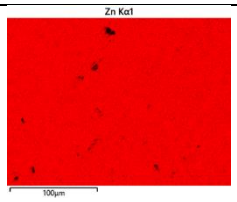	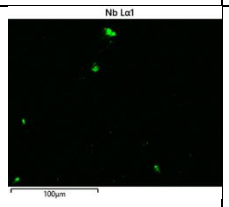	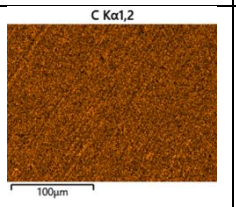	None Present
Bare Steel at 0 rpm	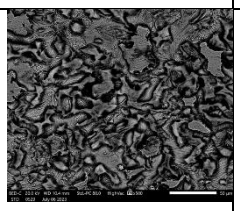	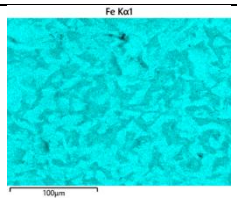	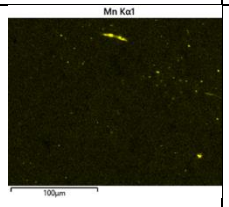	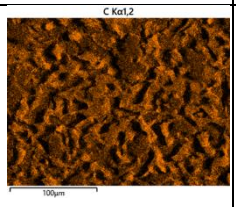	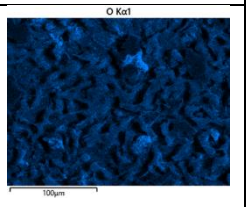
ZnNb Coating at 0 rpm	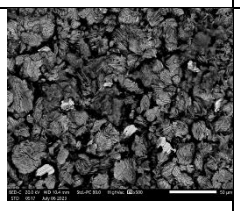	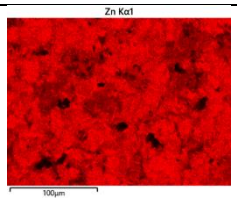	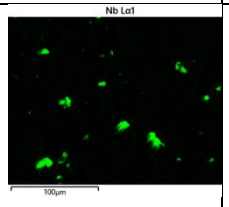	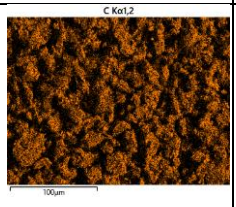	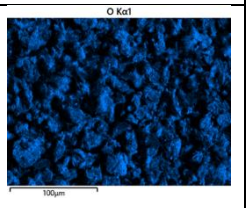
Bare Steel at 200rpm	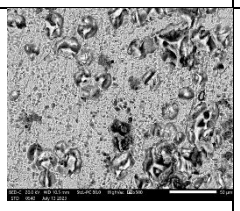	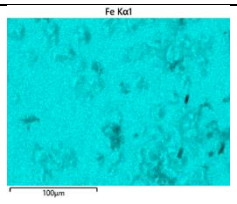	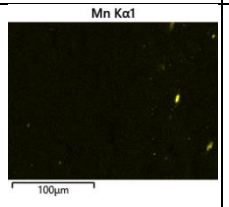	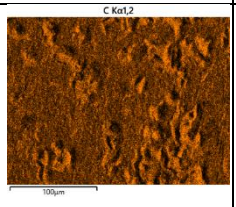	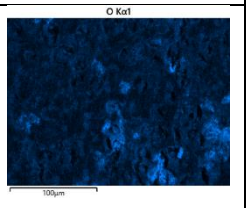
ZnNb at 200 rpm	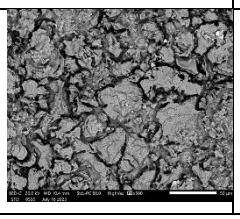	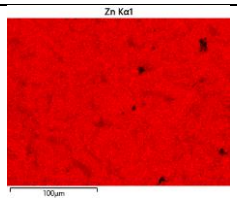	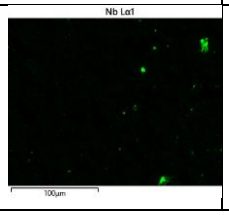	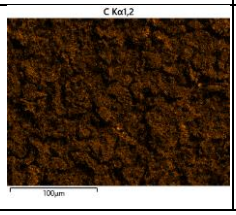	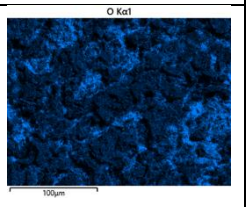

Figure 9: SEM images combined with associated EDS mappings of elements in corrosion samples. Elements by color: Iron (light blue), Zn (red), Mn (yellow), Nb (green), C (brown), and O (dark blue).

CONCLUSIONS

The electrochemical experiments completed in this study helped to understand the flow effect of a natural gas pipeline on CO_2 corrosion for uncoated and coated steel with ZnNb cold spray coating. The enclosed glass cell setup successfully created the conditions, simulating the pipeline's flow and CO_2 environment. The cold spray coating exhibited good behavior against corrosion under the flow compared to the steel with a fast passivation. The corrosion rate expected to increase underflow displayed the opposite trend for the coating but was still ambiguous between the two techniques used to measure this value. Further

exploration into the true nature of the effect on the mechanisms by flow is needed to understand this, such as the corrosion rate weight loss method. Further evaluation of the EIS data using models to follow the trends of individual components of each system will also help further understand what is to be expected for these conditions. Regardless, this coating does show promise with its ability to passivate and block corrosion as a candidate for protection to natural gas pipelines.

DISCLAIMER

This project was funded by the United States Department of Energy, National Energy Technology Laboratory, in part, through a site support contract. Neither the United States Government nor any agency thereof, nor any of their employees, nor the support contractor, nor any of their employees, makes any warranty, express or implied, or assumes any legal liability or responsibility for the accuracy, completeness, or usefulness of any information, apparatus, product, or process disclosed, or represents that its use would not infringe privately owned rights. Reference herein to any specific commercial product, process, or service by trade name, trademark, manufacturer, or otherwise does not necessarily constitute or imply its endorsement, recommendation, or favoring by the United States Government or any agency thereof. The views and opinions of authors expressed herein do not necessarily state or reflect those of the United States Government or any agency thereof.

ACKNOWLEDGEMENTS

This work was performed in support of the U.S. Department of Energy's (DOE) Office of Fossil Energy and Carbon Management's Emissions Mitigation Research Program and executed through the National Energy Technology Laboratory (NETL) Research & Innovation Center's Natural Gas Infrastructure Field Work Proposal and sponsored by the Mickey Leland Energy Fellowship. The authors of this project report would like to thank the technicians, Trevor Godell, Dennis Harvey, and Matthew Fortner, for their support in the laboratory.

REFERENCES

1. D. Justman, K. Rose, J. Bauer, NETL, 2017. Data analyzed from U.S. DOT PHMSA incident data.
2. Z. Belarbi; Richard. E. Chinn; Ö. N. Doğan, "Corrosion of zinc cold spray coatings in a wet sweet and sour gas environment," Corrosion 80,7 (2024): p.676.
3. S. Nesic, "Effects of multiphase flow on internal CO_2 corrosion of mild steel pipelines", Energy & Fuels 26,7 (2012): p. 4098.
4. Z. Belarbi, F. Farelas, M. Singer, S. Nesic, "Role of amines in the mitigation of CO_2 top-of-the-line corrosion", Corrosion 72,10 (2016): p. 1300.
5. Z. Belarbi, J.M. Dominguez Olivo, F. Farelas, M. Singer, D. Young, S Nesic, "Decanethiol as a corrosion inhibitor for carbon steels exposed to aqueous CO_2", Corrosion 75, 10 (2019): p. 246.
6. B.A.F. Santos, M.E.D. Serenario, R.C. Souza, J.R. Oliveira, G.L. Vaz, J.A.C.P. Gomes, A. H.S. Bueno, "The electrolyte renewal effect on the corrosion mechanisms of API X65 carbon steel under sweet and sour environments", Journal of Petroleum Science and Engineering 199, (2021): p.108347.
7. M. Singer, A. Camacho, B. Brown, and S. Nesic, "Sour top-of-the-line corrosion in the presence of acetic acid," Corrosion, 67, 8 (2011): p. 085003-1.
8. Z. Belarbi, F. Farelas, D. Young, M. Singer, S Nesic, "Effect of operating parameters on the inhibition efficacy of decanethiol", CORROSION/2018, paper no 10823 (Houston, TX: NACE, 2018).

9. Y. He, S. Ren, X. Wang, D. Young, M. Singer, Z. Belarbi, M. Mohamed-Saïd, S. Camperos, Md R. Khan, K. Cimatu, “Delinkage of metal surface saturation concentration and micellization in corrosion inhibition”, Corrosion 78, 7(2022): p. 625.
10. M. Matthew Ali, C. J. Magee, P. Y. Hsieh "Corrosion protection of steel with metal-polymer composite barrier liners," Journal of Natural Gas Science and Engineering 81, 103407 (2020): p. 1.
11. G. Siegmund, G. Schmitt, J. Noga, B. Sadlowsky, " Permeation damage of polymer liner in oil and gas pipelines: A Review" Polymer 12, 10 (2020): P.2307-1.
12. E. Lapushkina,” Anti-corrosion coatings fabricated by cold spray technique: Optimization of spray condition and the relationship between microstructure and performance Materials,” Université de Lyon; Tohoku Gakuin University (Sendai, Japon), 2020.
13. Z. Belarbi, R. E. Chinn, O. Dogan, “Corrosion of zinc cold spray coatings in a wet sweet and sour gas environment”, Corrosion 80, 7 (2024): p. 676.
14. L. Teeter, M. Z.-. Moroz, J. Tylczak and G. Crawford, " ZnCr and ZnNb cold spray coatings;” CORROSION/2021, paper no 16977 (Houston, TX: NACE, 2021).
15. Z. Belarbi, R. E. Chinn, O. Dogan, P. Carr, and J. Samson, " Field Testing of Self-Healing Metallic Coatings for Internal Corrosion Protection of Natural Gas Pipelines,” AMPP 2023, paper no 18857 (AMPP, 2023).
16. Belarbi, Zineb, Chinn, Richard E., Doğan, Ömer N., Carr, Patrick, and Samson, Julius. Field Testing of Self-Healing Metallic Coatings for Internal Corrosion Protection of Natural Gas Pipelines. United States: N. p., 2023. Web. doi:10.2172/1957980.
17. M. Cadorin, M. Morini*, M. Pinelli, “Numerical analyses of high Reynolds number flow of high-pressure fuel gas through rough pipes”, International Journal of Hydrogen Energy 35, (2010): p. 7568.
18. E. S. MENON, “Transmission pipeline calculations, and simulations manual,” (Oxford: Elsevier Inc., 2015).
19. S. Nes˘ic´, G.T. Solvi, J. Enerhaug, “Comparison of the rotating cylinder and pipe flow tests for flow-sensitive carbon dioxide corrosion”, Corrosion 51, 10 (1995): p. 773.
20. S. Nesic, “Key issues related to modeling of internal corrosion of oil and gas pipelines – A review”, Corrosion Science 49, (2007): p. 4308.
21. Z. Belarbi, D.A. Daramola, J. P. Trembly, “Bench-scale demonstration and thermodynamic simulations of electrochemical nutrient reduction in wastewater via recovery as struvite,” Journal of The Electrochemical Society 167, 15 (2020): p. 155524.
22. Z. Belarbi, F. Farelas, D. Young, M. Singer, "Effect of steel microstructure and corrosion product characteristics on inhibition performance of decanethiol against top-of-the-line corrosion" , CORROSION /2021, paper no 16581 (Houston, TX: NACE, 2021).